Monthly Notices
of the
ROYAL ASTRONOMICAL SOCIETY

Mon. Not. R. Astron. Soc. **418,** 906–915 (2011) doi:10.1111/j.1365-2966.2011.19541.x

Suppression and spatial variation of early galaxies and minihaloes

Dmitriy Tseliakhovich,[1]★ Rennan Barkana[2] and Christopher M. Hirata[3]

[1]*California Institute of Technology, MC 249-17, 1200 East California Boulevard, Pasadena, CA 91125, USA*
[2]*Raymond and Beverly Sackler School of Physics and Astronomy, Tel Aviv University, Tel Aviv 69978, Israel*
[3]*California Institute of Technology, MC 350-17, 1200 East California Boulevard, Pasadena, CA 91125, USA*

Accepted 2011 July 28. Received 2011 July 21; in original form 2010 December 12

ABSTRACT

We study the effect of the relative velocity of dark matter and baryonic fluids after the epoch of recombination on the evolution of the first bound objects in the early Universe. Recent work has shown that, although the relative motion of the two fluids is formally a second-order effect in density, it has a dramatic impact on the formation and distribution of the first cosmic structures. Focusing on the gas content, we analyse the effect of relative velocity on the properties of haloes over a wide range of halo masses and redshifts. We accurately calculate the linear evolution of the baryon and dark matter fluctuations, and quantify the resulting effect on haloes based on an analytical formalism that has been carefully checked with simulations in the case with no relative velocity. We estimate the effect on the abundance of early haloes and the gas fraction in them. We find that the relative velocity effect causes several changes: (i) the characteristic mass that divides gas-rich and gas-poor haloes is increased by roughly an order of magnitude, from 2×10^4 to about $2 \times 10^5\,\mathrm{M}_\odot$; (ii) this characteristic mass has a large scatter (full width at half-maximum $\sim 1.5 \times 10^5\,\mathrm{M}_\odot$ at $z = 20$); (iii) the fraction of baryons in star-less minihaloes is suppressed by a factor of 3.3 at $z = 20$; (iv) the fraction of baryons in haloes that can cool and form stars is suppressed by a factor of 1.5 at $z = 20$; and (v) there are enhanced spatial variations of these various fractions.

Key words: dark ages, reionization, first stars – large-scale structure of Universe.

1 INTRODUCTION

One of the most important questions in astrophysics today is understanding the formation and evolution of the first bound structures. This question is actively studied today through theoretical and observational work as well as through advanced numerical simulations. Significant theoretical and observational efforts are devoted to understanding properties of the first galaxies and minihaloes, at what redshifts they form and how they influence the epoch of reionization. Observations, most notably of the cosmic microwave background (CMB), have established the basic parameters for the initial conditions of structure formation (Bennett et al. 2003), thus providing a foundation for theoretical work on the first structures. Recent advances in computation have made it possible to simulate the formation of the first stars and early galaxies (Abel, Bryan & Norman 2002; O'Shea et al. 2005; Yoshida, Omukai & Hernquist 2008; Stacy, Greif & Bromm 2010; Clark et al. 2011). Meanwhile, several efforts are underway to probe the structure of the intergalactic medium during the reionization epoch using the 21-cm line of hydrogen, and second-generation experiments may be able to explore the early stages of reionization.

In studying the formation of the first structures, it is convenient to identify two major classes of the early-type objects. The first class consists of large haloes in which the gas can cool and form stars. These haloes are the presumed sites of the first dwarf galaxies, which produce the first sources of metals in the Universe, and provide ultraviolet photons that begin the decoupling of the hydrogen spin temperature from the CMB (Madau, Meiksin & Rees 1997), eventually starting the epoch of reionization. The second class consists of smaller haloes ('minihaloes') that are too small for molecular cooling, but still affect the epoch of reionization by acting as sinks for ionizing photons (Haiman, Abel & Madau 2001; Barkana & Loeb 2002; Ciardi et al. 2005; Iliev, Scannapieco & Shapiro 2005) and may generate a 21-cm signal from collisional excitations of hydrogen (e.g. Iliev et al. 2003; Furlanetto & Oh 2006). It is important to understand both the abundance and the distribution of haloes, as well as the precise boundaries separating haloes that undergo cooling and star formation, those that collect baryons in their potential wells but do not cool, and the lightest haloes that exist only as dark matter structures and do not collect gas.

In this work, we study the formation of the first galaxies and minihaloes in light of an important effect of the relative velocity of dark matter and baryonic fluids (Tseliakhovich & Hirata 2010) that was previously overlooked. This effect leads to the

★E-mail: dimlyus@caltech.edu

suppression of power on scales corresponding to the first bound haloes ($M_{\rm h} \sim 10^4$–$10^8\,{\rm M}_\odot$) and delays the formation of the first objects. More importantly, this effect introduces scale-dependent bias and stochasticity, leading to significant qualitative changes in the distribution of the first objects. The relative velocity effect is especially important on the small scales where the first stars and galaxies form. Introduction of this effect dramatically changes the gas distribution inside the first haloes and changes the characteristic mass of gas-rich objects. Dalal, Pen & Seljak (2010) recently calculated analytically the effect on the gas content of haloes and found a large effect on the fluctuations of the Lyman α background at high redshifts. Their analysis, however, was based on a very simplified model of which haloes can form stars and in what abundance. In this paper, we carry out a detailed analytical study of the distribution of gas and stars in the first haloes.

Furthermore, in this study, we use a more robust set of initial conditions compared to Tseliakhovich & Hirata (2010) and remove a number of simplifying assumptions. We emphasize an important role of proper initial conditions, following a detailed study by Naoz, Yoshida & Barkana (2010) who showed that three commonly used initial condition setups lead to significantly different abundances and properties of the first star-forming gas clouds as well as the first minihaloes.

The rest of this paper is organized as follows. Section 2 reviews the relative velocity effect (Section 2.1) and improves the analysis of Tseliakhovich & Hirata (2010) to account for spatial variation of the sound speed (Section 2.2). Section 3 then investigates the early haloes and their gas content, focusing on the computation of the filtering mass (Section 3.1) and then examining the fraction of baryons in minihaloes and in larger haloes that can cool, including an analysis of spatial variations in the baryon budget (Sections 3.2 and 3.3). We summarize our results in Section 4 and compare them to other recent works.

The numerical results and plots shown in this paper assume a cosmology with present-day baryon density $\Omega_{\rm b,0} = 0.044$, cold dark matter (CDM) density $\Omega_{\rm c,0} = 0.226$, dark energy density $\Omega_{\Lambda,0} = 0.73$, Hubble constant $H_0 = 71\ {\rm km\,s^{-1}\,Mpc^{-1}}$, and adiabatic primordial perturbations of variance $\Delta^2_\zeta(k_\star) = 2.42 \times 10^{-9}$ at $k_\star = 0.002\,{\rm Mpc}^{-1}$, with slope $n_{\rm s} = 0.96$.

2 INITIAL CONDITIONS FOR HALO FORMATION

In this section, we detail the formalism necessary for the generation of correct initial conditions, taking into account two important effects that are often overlooked in the literature. First of all, we introduce the effect of relative velocity of dark matter and baryonic fluids after recombination. This effect, first studied in Tseliakhovich & Hirata (2010), is nominally a second-order effect in the perturbation theory of density evolution and hence has been ignored in studies based on the linear theory. Secondly, we emphasize the importance of a correct treatment of the sound speed variations in the time between recombination and $z \sim 200$ due to residual Compton heating of the electrons on the CMB photons. As we show later in this paper, both effects play a significant role during the epoch of first halo formation and dramatically impact gas fractions in the first bound objects.

2.1 Relative velocity of dark matter and baryonic fluids

Before recombination, the baryons are tightly coupled to the photons, and the sound speed is highly relativistic, $c_{\rm s} \sim c/\sqrt{3}$. As the universe expands and cools, the electrons recombine with the protons and the Universe becomes transparent, leading to a kinematic decoupling of the baryons from the radiation around $z_{\rm dec} \approx 1000$. After recombination, the sound speed of the baryons drops precipitously down to thermal velocities, whereas the dark matter velocity remains unaffected, and after recombination, the dark matter motion with respect to the baryons becomes supersonic. The relative velocity can be written as

$$\boldsymbol{v}_{\rm bc}(\boldsymbol{k}) = \frac{\hat{\boldsymbol{k}}}{{\rm i}k}[\theta_{\rm b}(\boldsymbol{k}) - \theta_{\rm c}(\boldsymbol{k})], \tag{1}$$

where $\hat{\boldsymbol{k}}$ is a unit vector in the direction of the wavevector $\boldsymbol{k}$, and $\theta \equiv a^{-1}\nabla \cdot \boldsymbol{v}$ is the velocity divergence (we use comoving coordinates).

The variance of this relative velocity is

$$\begin{aligned}\langle v^2_{\rm bc}(\boldsymbol{x})\rangle &= \int \frac{{\rm d}k}{k}\Delta^2_\zeta(k)\left[\frac{\theta_{\rm b}(k) - \theta_{\rm c}(k)}{k}\right]^2 \\ &= \int \frac{{\rm d}k}{k}\Delta^2_{\rm vbc}(k),\end{aligned} \tag{2}$$

where $\Delta^2_\zeta(k) = 2.42 \times 10^{-9}$ is the initial curvature perturbation variance per $\ln k$. Integration of equation (2) at the time of recombination[1] ($z_{\rm rec} = 1020$) shows that the dark matter moves relative to the baryons with rms velocity $\sim 30\,{\rm km\,s^{-1}}$ corresponding to a Mach number of $\mathcal{M} \equiv v_{\rm bc}/c_{\rm s} \sim 5$. This supersonic relative motion allows baryons to advect out of the dark matter potential wells and significantly suppresses the growth of structure at wavenumbers higher than

$$k_{\rm vbc} \equiv \left.\frac{aH}{\langle v^2_{\rm bc}\rangle^{1/2}}\right|_{\rm dec} = \frac{k_{\rm J}}{\mathcal{M}} \sim 40\,{\rm Mpc}^{-1}, \tag{3}$$

where $k_{\rm J}$ is the Jeans wavenumber.

As shown in Tseliakhovich & Hirata (2010), the relative velocity of the baryons and CDM is coherent over scales of several comoving Mpc and the velocity in each coherence region is well described by a three-dimensional Gaussian probability distribution with variance

$$\sigma^2_{\rm vbc} = \left\langle |\boldsymbol{v}_{\rm bc}(\boldsymbol{x})|^2 \right\rangle. \tag{4}$$

(Note that this is the *total* variance, that is, including velocities in all three directions; the variance per axis is smaller by a factor of 3.)

To see how the relative motion of baryons and dark matter affects the formation of the first objects, we need to solve a system of evolution equations that incorporate this effect. The system of equations describing a high-k perturbation mode in the presence of a background relative velocity is

$$\begin{aligned}\frac{\partial\delta_{\rm c}}{\partial t} &= \frac{\rm i}{a}\boldsymbol{v}^{\rm (bg)}_{\rm bc}\cdot\boldsymbol{k}\delta_{\rm c} - \theta_{\rm c}, \\ \frac{\partial\theta_{\rm c}}{\partial t} &= \frac{\rm i}{a}\boldsymbol{v}^{\rm (bg)}_{\rm bc}\cdot\boldsymbol{k}\theta_{\rm c} - \frac{3H^2}{2}(\Omega_{\rm c}\delta_{\rm c} + \Omega_{\rm b}\delta_{\rm b}) - 2H\theta_{\rm c}, \\ \frac{\partial\delta_{\rm b}}{\partial t} &= -\theta_{\rm b}\end{aligned}$$

and

$$\frac{\partial\theta_{\rm b}}{\partial t} = -\frac{3H^2}{2}(\Omega_{\rm c}\delta_{\rm c} + \Omega_{\rm b}\delta_{\rm b}) - 2H\theta_{\rm b} + \frac{c_{\rm s}^2k^2}{a^2}\delta_{\rm b}. \tag{5}$$

The $v_{\rm bc}$ terms are nominally of second order in perturbation theory, and hence one may wonder why they, rather than other

[1] Technically, the effective redshift of kinematic decoupling (Eisenstein & Hu 1998) since recombination is an extended process.

second-order terms, are included. The reason is that the expansion parameter for these terms is not the density perturbation δ, but rather the ratio of the advection terms [e.g. $v_{\rm bc}^{\rm (bg)} k\delta_{\rm c}/a$ in the $\delta_{\rm c}$ equation] to the linear terms (e.g. $\partial\delta_{\rm c}/\partial t \sim \delta_{\rm c}/H$). This ratio is

$$\frac{v_{\rm bc}^{\rm (bg)} k}{aH}. \tag{6}$$

One can see that this expansion parameter increases as one goes to smaller scales and is of the order of unity at $k \sim k_{\rm vbc}$. Thus, the $v_{\rm bc}$ terms become non-perturbative at small scales $k > k_{\rm vbc}$, and when treating these small scales, one must keep these terms even if they are formally of higher order in the perturbation theory.

2.2 Complete heating model

The system of equations (5) assume a spatially uniform sound speed which is a good first-order approximation. However, as shown in Naoz & Barkana (2005), they underestimate baryon density fluctuations by more than 30 per cent at $z = 100$ and 10 per cent at $z = 20$ for large wavenumbers. A fully correct treatment of baryon density evolution requires analysis of the Compton heating from the CMB on the sound speed and fluctuations in the temperature distribution. Following Naoz & Barkana (2005), we rewrite the sound speed term of the last equation of equation (5) as

$$\frac{c_{\rm s}^2 k^2}{a^2}\delta_{\rm b} \rightarrow \frac{k^2}{a^2}\frac{k_{\rm B}\bar{T}}{c^2\mu m_{\rm H}}(\delta_{\rm b} + \delta_T), \tag{7}$$

where δ_T is the temperature perturbation which evolves as

$$\frac{{\rm d}\delta_T}{{\rm d}t} = \frac{2}{3}\frac{{\rm d}\delta_{\rm b}}{{\rm d}t} + \frac{x_{\rm e}(t)}{t_\gamma}a^{-4}\left[\delta_\gamma\left(\frac{\bar{T}_\gamma}{\bar{T}} - 1\right) + \frac{\bar{T}_\gamma}{\bar{T}}\left(\delta_{T_\gamma} - \delta_T\right)\right]. \tag{8}$$

The second term on the right-hand side accounts for the Compton scattering of the CMB photons on the residual electrons from recombination. Here $x_{\rm e}(t)$ is the electron fraction relative to the total number density of gas particles,[2] $\bar{T}_\gamma = [2.725\ {\rm K}]/a$ is the mean CMB temperature and

$$t_\gamma^{-1} \equiv \frac{8}{3}\rho_\gamma^0\frac{\sigma_{\rm T}c}{m_{\rm e}} = 8.55 \times 10^{-13}\ {\rm yr}^{-1}, \tag{9}$$

where $\sigma_{\rm T}$ is the Thomson scattering cross-section, ρ_γ^0 is the photon energy density at $z = 0$ and $\bar{T}$ is the average temperature of the baryons, which can be calculated using the first law of thermodynamics:

$$\frac{{\rm d}\bar{T}}{{\rm d}t} = -2H\bar{T} + \frac{x_{\rm e}(t)}{t_\gamma}(\bar{T}_\gamma - \bar{T})\,a^{-4}. \tag{10}$$

Accounting for the Compton heating of the residual electrons by the CMB photons is especially important on small scales ($k > 1\ {\rm Mpc}^{-1}$), which are also impacted by the relative motion effect.

3 FIRST HALOES AND THEIR GAS CONTENT

Both of the effects discussed above have a significant impact on the evolution of density perturbations on small scales and affect the formation of the first dark matter haloes, as well as the subsequent accretion of the baryons and the formation of the first stars. We investigate the specific effects by studying the change in the characteristic mass scale that divides gas-rich and gas-poor haloes produced by the relative velocity of the dark matter and baryonic fluids.

[2] This is different from the recombination literature, which often takes $x_{\rm e}$ to be normalized to the number of hydrogen nuclei. At low redshifts, these differ by 8 per cent due to the presence of helium.

3.1 Filtering mass

In the ΛCDM universe, virialized dark matter haloes form hierarchically on extremely small scales at very early times and start accreting baryons into their potential wells. If haloes are heavy enough, accretion proceeds to the point where baryons start cooling through molecular line emission, condensing into the first stars and galaxies. This accretion is counteracted by the bulk motion of baryons with respect to dark matter as well as by the thermal gas pressure. The combination of the two effects leads to the presence of the minimal halo mass scale at which baryons are still able to effectively accrete on to a halo.

To study the effect of halo formation and baryonic accretion, it is convenient to consider a large ensemble of patches of the size of the relative velocity coherence scale (∼3 Mpc across). Each patch has certain mean density and bulk velocity, determined by linear initial conditions at the time of recombination. The bulk velocity for each patch is drawn from a Gaussian random distribution with the variance determined by equation (4), and the initial density power spectrum is generated using CMBFAST (Seljak & Zaldarriaga 1996). We follow the evolution of density perturbations in each patch from the time of recombination to some later redshift z, including the relative velocity effect as well as the spatial variation of the baryonic speed of sound due to Compton heating from the CMB (Naoz & Barkana 2005).

By evolving the system of equations (5) with the correct sound speed term of equation (7) in each patch, characterized by a fixed value of $v_{\rm bc}$, we calculate the baryonic and dark matter power spectra. Their ratio is constant on large scales (small k) and drops at high k due to the suppression of growth by the baryonic pressure. Gnedin & Hui (1998) originally defined a 'filtering' scale (essentially a time-averaged Jeans scale) that they used to identify the largest scale on which the baryon fluctuations are substantially suppressed compared to those of the dark matter. We use the generalized definition from Naoz & Barkana (2007), in which the baryon-to-total ratio is expanded to linear order in k^2 and written in the following form:

$$\frac{\delta_{\rm b}}{\delta_{\rm tot}} = 1 - \frac{k^2}{k_{\rm F}^2} + r_{\rm LSS}. \tag{11}$$

Here $\delta_{\rm tot} = f_{\rm b}\delta_{\rm b} + f_{\rm dm}\delta_{\rm dm}$ is the total density perturbation described in terms of the cosmic baryon and dark matter mass fractions, $f_{\rm b}$ and $f_{\rm dm}$, and the k-independent $r_{\rm LSS}$ term (which is negative) describes the relative baryon-to-total difference in the limit of large-scale structure, that is, where both the $v_{\rm bc}$ effect and the thermal pressure of the gas are negligible (and restricted also to scales below the baryon acoustic oscillations).

In Fig. 1, we plot isotropically the averaged perturbation ratio $\delta_{\rm b}/\delta_{\rm tot}$ by averaging over the direction of $\boldsymbol{k}$ with respect to $\boldsymbol{v}_{\rm bc}$. On large scales, the ratio is very close to constant, and using equation (11), we can deduce the value of $r_{\rm LSS}$ at various redshifts. For example, $r_{\rm LSS} = -0.054$ at $z = 20$. The filtering scale $k_{\rm F}$ is obtained by fitting equation (11) to the calculated values of the ratio $\delta_{\rm b}/\delta_{\rm tot}$ from Fig. 1. This allows us to define the filtering mass in terms of the filtering wavenumber:

$$M_{\rm F} = \frac{4\pi}{3}\bar{\rho}_0\left(\frac{\pi}{k_{\rm F}}\right)^3, \tag{12}$$

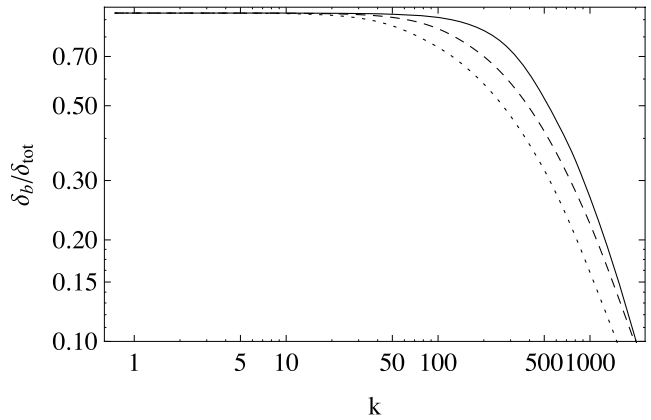

Figure 1. Perturbation ratio δ_b/δ_{tot} versus comoving wavenumber k evaluated at $z = 20$ for the cases of $v_{bc} = 0$ (solid curve), $v_{bc} = 1\sigma_{vbc}$ (dashed curve) and $v_{bc} = 2\sigma_{vbc}$ (dotted curve). In all cases, overdensities are isotropically averaged over the direction of $\boldsymbol{k}$ with respect to $\boldsymbol{v}_{bc}$.

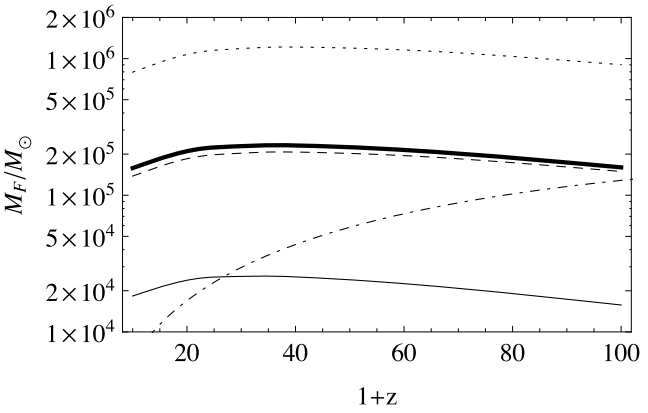

Figure 2. Evolution of the filtering mass with redshift in the regions with $v_{bc} = 0$ (thin solid line), $v_{bc} = 1\sigma_{vbc}$ (dashed line), $v_{bc} = 2\sigma_{vbc}$ (dotted line) and in the global average case (thick solid line). We also show the evolution of the Jeans mass M_J (dot–dashed line).

where $\bar{\rho}_0$ is the mean matter density today. We note that this relation is one-eighth of the definition originally used by Gnedin (2000) who also used a non-standard definition of the Jeans mass.

The filtering mass plays an extremely important role in understanding the evolution of the first haloes, as it provides a good approximation for the boundary between gas-rich haloes and haloes that do not contain substantial quantities of gas. Traditionally, one would assume that the separation between gas-rich and gas-poor objects is represented by the Jeans scale, which is the minimum scale on which a small gas perturbation will grow due to gravity overcoming the pressure gradient. However, the Jeans scale is related only to the evolution of the perturbations at a given point in time and does not account for significant variation in the Jeans mass with time. The filtering mass, on the other hand, reflects the baryonic pressure effects integrated over the entire history of the Universe, and provides a much better approximation to the boundary between gas-rich and gas-poor haloes.

An extensive study of the filtering mass properties and evolution history in models without the relative velocity effect was performed in Naoz & Barkana (2005) and Naoz & Barkana (2007). The properties of the filtering mass, however, are significantly modified in the regions where the bulk motion of baryons with respect to dark matter potential wells is significant. In regions with high values of v_{bc}, baryons tend to advect out of the collapsing dark matter haloes, significantly increasing the filtering mass. We demonstrate this in Fig. 2 where we plot the evolution of the filtering mass with redshift in the regions with $v_{bc}/\sigma_{vbc} = 0$, 1 and 2. We also show the globally averaged case by integrating the filtering mass over the full probability distribution of the relative velocity, given by:[3]

$$P_{vbc}(v) = \left(\frac{3}{2\pi\sigma_{vbc}^2}\right)^{3/2} 4\pi v^2 \exp\left(-\frac{3v^2}{2\sigma_{vbc}^2}\right). \quad (13)$$

As noted earlier, the variance per axis is $\sigma_{vbc}^2/3$.

[3] This is the distribution of the magnitude of $\boldsymbol{v}_{bc}$, where the vector $\boldsymbol{v}_{bc}$ is the result of linear perturbations and hence is drawn from a multivariate Gaussian. It thus happens to be the same as the Maxwell–Boltzmann distribution, even though the bulk velocities of baryons have nothing to do with thermal motions of particles.

In Fig. 2, we also compare the filtering mass with the Jeans mass defined as

$$M_J = \frac{4\pi}{3}\bar{\rho}_0\left(\frac{\pi}{k_J}\right)^3, \quad (14)$$

where $k_J = \sqrt{2/3}aH/c_s$ is the Jeans scale [defined by setting the right-hand side of equation (5) to zero, without the relative velocity term, and neglecting here the correction of equation (7)]. Fig. 2 shows that the filtering mass reaches a maximum value at redshift $z \sim 40$ (and generally varies only slightly throughout the plotted redshift range), whereas the Jeans mass continuously decreases with time due to the drop in the sound speed of the gas as the Universe cools.

The filtering mass represents a time-averaged Jeans mass and hence it decreases at the low redshifts; however, right after recombination, baryonic perturbations on small scales are highly suppressed and they only catch up gradually, causing the filtering mass to increase from low initial values. We emphasize that in the regions with a high value of the relative velocity, the filtering mass is significantly larger than in the regions with small values of v_{bc} and hence the formation of gas-rich objects in those regions proceeds quite differently from that in the regions with $v_{bc} \sim 0$. The filtering scale and mass [from equations (11) and (12)] in regions with varying values of v_{bc} are given in Table 1, and the filtering masses at $z = 20$ and 40 are plotted in Fig. 3. In Fig. 4, we also show the dependence of the filtering mass on the angle θ between the direction of $\boldsymbol{v}_{bc}$ and that of the wavevector $\boldsymbol{k}$ in regions where $v_{bc} = 1\sigma_{vbc}$ at $z = 20$; the plot shows that the main contribution to the filtering mass comes from the regions where the wavenumber $\boldsymbol{k}$ and the relative velocity vector $\boldsymbol{v}_{bc}$ are parallel (or antiparallel).

Table 1. Filtering scale and filtering mass for the isotropic averaging of the direction of $\boldsymbol{k}$ with respect to $\boldsymbol{v}_{bc}$ at $z = 20$.

$v_{bc}/\sigma_{v_{bc}}$	$P(> v_{bc})$	k_F (Mpc^{-1})	M_F ($M_\odot$)
4	2.1×10^{-10}	85	7.75×10^6
3	5.9×10^{-6}	113	3.37×10^6
2	7.4×10^{-3}	166	1.07×10^6
1	0.392	298	1.85×10^5
0	1	591	2.39×10^4

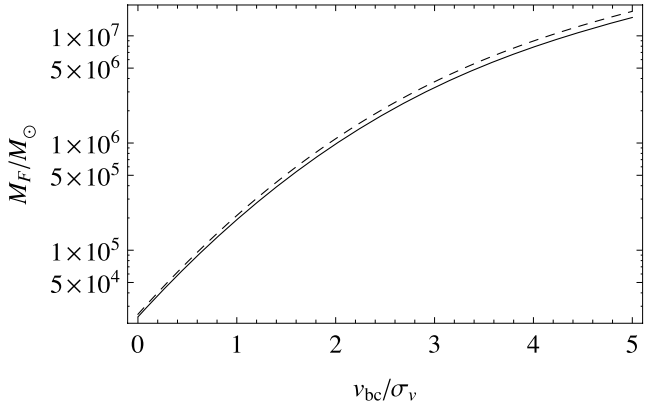

Figure 3. This figure shows the filtering mass M_F as a function of the relative velocity of the dark matter and baryonic fluids at $z = 20$ (solid line) and $z = 40$ (dashed line).

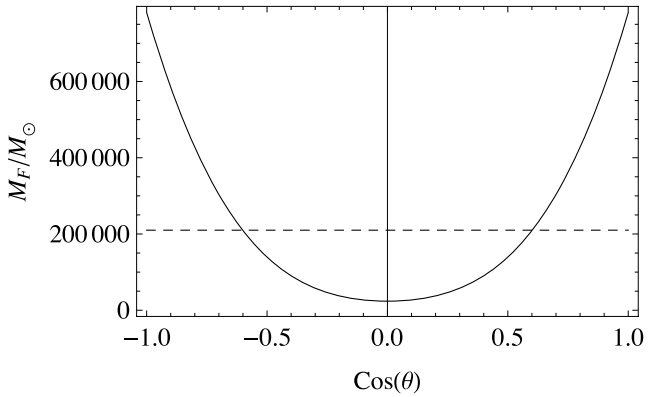

Figure 4. The lower panel shows the dependence of the filtering mass on the angle θ between the directions of $\boldsymbol{v}_{bc}$ and the wavevector $\boldsymbol{k}$ (solid line), and the isotropically averaged value of M_F (dashed horizontal line), in regions where $v_{bc} = 1\sigma_{vbc}$ at $z = 20$.

3.2 Gas content of the first galaxies and minihaloes

We now investigate the amount of gas that falls into early haloes, and how much of this gas is capable of cooling. Here we use analytical approximations – namely the relation between the gas mass fraction f_g and the filtering mass M_F, and the Sheth & Tormen (1999) mass function – that have been calibrated against simulations with statistically isotropic initial conditions and no bulk relative velocity. In our case with $v_{bc} \neq 0$, the power spectra are both reduced and slightly anisotropic, but we expect these approximations to still be a useful guide since statistical anisotropy (e.g. θ-dependent filtering mass) can only appear at second order in scalars such as the halo mass function or gas content.

There is no a priori reason to suppose that the filtering mass, which is defined based on linear perturbations, can also accurately describe properties of highly non-linear, virialized objects. Qualitatively, we may argue that if pressure significantly opposes gravity during the halo formation process (which for some time is accurately described by linear theory), then it will significantly suppress the amount of gas in the final virialized halo. Gnedin (2000) suggested, based on simulations during cosmic reionization, that the filtering mass accurately fits the mass for which a halo contains half the mean cosmic baryon fraction f_b, and fitted the simulation results to the following formula:

$$f_g = f_{b,0}\left[1 + \left(2^{\alpha/3} - 1\right)\left(\frac{M_F}{M}\right)^{\alpha}\right]^{-3/\alpha}, \quad (15)$$

where $f_{b,0}$ is the gas fraction in the high-mass limit. In this function, a higher α causes a sharper transition between the high-mass limit (constant f_g) and the low-mass limit (assumed to be $f_g \propto M^3$). This formula has subsequently been found to agree with hydrodynamic simulations (Naoz, Barkana & Mesinger 2009; Naoz et al. 2010) if we set $\alpha \approx 0.7$ and $f_{b,0} = f_b(1 + 3.2r_{LSS})$ (Barkana & Loeb 2011), and use the filtering mass as defined in equation (12) (which differs from Gnedin 2000, as noted earlier). Thus, at each redshift, in each patch of the Universe we may calculate the local value of M_F and from it the gas fraction in haloes of various total masses. In Fig. 5, we plot the gas fraction as a function of halo mass in regions with varying values of relative velocity at $z = 20$. It is clear that haloes that would be gas rich in the Universe with no v_{bc} effect become gas poor in the regions where the relative velocity is high. We also see that, on average, introduction of the v_{bc} effect significantly lowers the gas fraction in all haloes with $M_h < 10^7\,M_\odot$.

In order to find the total amount of gas in galaxies, we must integrate over the halo mass function in each patch. We start with the $v_{bc} = 0$ case. Standard models for halo formation are based on spherical collapse calculations, in which the linear overdensity must reach a critical threshold $\delta_c(z)$ for the corresponding region to form a collapsed halo at redshift z. The halo abundance depends on the statistics of fluctuations on various scales, which can be parametrized by the function $S(R)$, the variance of fluctuations in spheres of radius R (S is also a function of redshift). $S(R)$ can be written as

$$S(R) = \int \Delta^2_m(k)|W(k, R)|^2 \frac{dk}{k}, \quad (16)$$

where $\Delta^2_m(k)$ is the isotropically averaged local matter power spectrum and $W(k, R)$ is the window function corresponding to spheres of radius R.

We define $f(\delta_c(z), S)dS$ to be the mass fraction contained at z within haloes with masses in the range corresponding to S to $S + dS$. We convert between halo mass M and (initial comoving) radius R using the cosmic mean density: $M = \frac{4}{3}\pi R^3\bar{\rho}_0$. The halo abundance

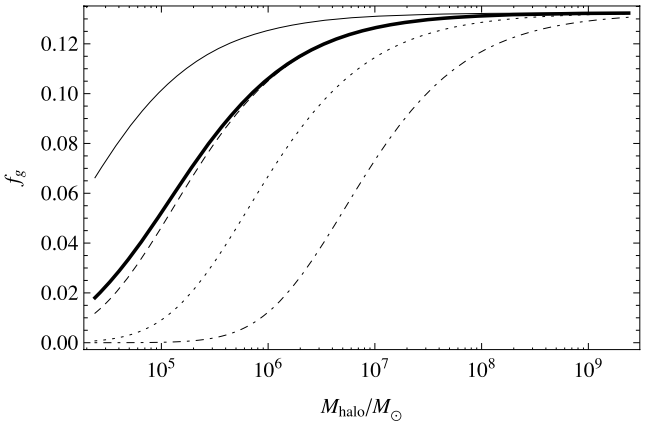

Figure 5. Change in the gas fraction f_g at $z = 20$ as a function of halo mass for regions with $v_{bc} = 0$ (thin solid line), $v_{bc} = 1\sigma_{vbc}$ (dashed line), $v_{bc} = 2\sigma_{vbc}$ (dotted line), $v_{bc} = 4\sigma_{vbc}$ (dot–dashed line) and for the isotropically averaged case (thick solid line, nearly coincident with the dashed line above $M_h \sim 10^6\,M_\odot$).

is then

$$\frac{\mathrm{d}n}{\mathrm{d}M} = \frac{\bar{\rho}_0}{M}\left|\frac{\mathrm{d}S}{\mathrm{d}M}\right| f(\delta_\mathrm{c}(z), S), \tag{17}$$

where dn is the comoving number density of haloes with masses in the range M to $M + \mathrm{d}M$. In the model of Press & Schechter (1974),

$$f_\mathrm{PS}(\delta_\mathrm{c}(z), S) = \frac{1}{\sqrt{2\pi}}\frac{\nu}{S}\mathrm{e}^{-\nu^2/2}, \tag{18}$$

where $\nu = \delta_\mathrm{c}(z)/\sqrt{S}$ is the number of standard deviations that the critical collapse overdensity represents on the mass scale M corresponding to the variance S.

However, the Press–Schechter mass function fits numerical simulations only qualitatively, and in particular it substantially underestimates the abundance of the rare haloes that host galaxies at high redshift. The halo mass function of Sheth & Tormen (1999), which fits numerical simulations much more accurately, is given by

$$f_\mathrm{ST}(\delta_\mathrm{c}(z), S) = A'\frac{\nu}{S}\sqrt{\frac{a'}{2\pi}}\left[1 + \frac{1}{(a'\nu^2)^{q'}}\right]\mathrm{e}^{-a'\nu^2/2}, \tag{19}$$

with the best-fitting parameters (Sheth & Tormen 2002) $a' = 0.75$ and $q' = 0.3$, and where the normalization to unity is ensured by taking $A' = 0.322$.

The critical density of collapse $\delta_\mathrm{c}(z)$ is independent of mass and equals 1.69 in the Einstein–de Sitter limit, valid over a wide range of redshifts. Its value decreases at low redshift due to the cosmological constant, but more relevant for this paper is the decrease at very high redshift due to the effects of the baryons and radiation. The decrease is by $\sim 0.05(1+z)$ per cent from the Einstein–de-Sitter value (Naoz, Noter & Barkana 2006; Naoz & Barkana 2007), a small effect that is, however, greatly amplified by the fact that galaxies at the highest redshifts form in haloes that correspond to very rare density fluctuations.

In our approach, we must calculate how the halo mass function varies in different regions. The Press–Schechter model has been extended (Bond et al. 1991) to describe the variation in the halo abundance in regions of various density, and we can generalize this to include the bulk velocity by including the variation in the function $S(R)$ with v_bc. To demonstrate this dependence, we plot in Fig. 6 $\sqrt{S} \equiv \sigma(v_\mathrm{bc}|M_\mathrm{h})$ as a function of the relative velocity at a fixed halo mass M_h. We see that the variance of the density perturbations decreases with increasing v_bc, leading to a delay in the collapse of dark matter haloes. We also find that the change in σ is larger for haloes of low mass since the power spectrum on scales much larger than the filtering mass is unaffected by the relative velocity.

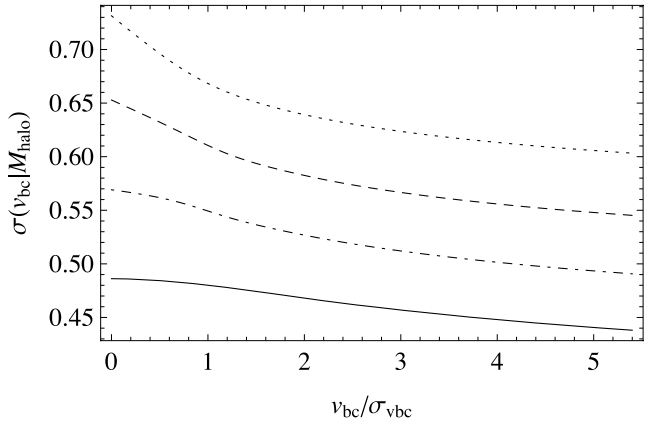

Figure 6. Dependence of $\sigma(v_\mathrm{bc}|M_\mathrm{h})$ on the relative velocity v_bc at $z = 20$ for a fixed mass of the collapsed haloes: $M_\mathrm{h} = 10^7$ (solid line), 10^6 (dot–dashed line), 10^5 (dashed line) and 10^4 $\mathrm{M}_\odot$ (dotted line).

We can summarize the important effects of the change in halo abundance and halo gas content at a given mass scale by calculating various gas fractions at each redshift. This can be done by using the Sheth–Tormen mass function and accounting for the changes due to the relative velocity effect. We calculate the fraction of the total matter density in haloes above a certain mass scale by

$$f_\mathrm{tot}(>M_\mathrm{h}) = \int_{M_\mathrm{h}}^{\infty}\frac{M}{\bar{\rho}_0}\frac{\mathrm{d}n}{\mathrm{d}M}\mathrm{d}M, \tag{20}$$

and the fraction of the baryon density contained in those haloes using equation (15):

$$f_\mathrm{gas}(>M_\mathrm{h}) = \int_{M_\mathrm{h}}^{\infty}\frac{M}{\bar{\rho}_0}\frac{\mathrm{d}n}{\mathrm{d}M}\frac{f_\mathrm{g}}{f_\mathrm{b}}\mathrm{d}M. \tag{21}$$

We plot both fractions in Fig. 7 at $z = 20$ for $v_\mathrm{bc}/\sigma_\mathrm{vbc} = 0$, 1 and 2, and for the globally averaged case, where we take into consideration the global distribution of v_bc. The plot clearly shows that in regions with high relative velocity, the gas fraction in haloes is dramatically suppressed. The global average (which comes out very close to the $v_\mathrm{bc}/\sigma_\mathrm{vbc} = 1$ case) gives a suppression by a factor of 2.3 of the total gas fraction in haloes. In order to separate out the various effects, we plot one case in which we use the correct halo mass function (as

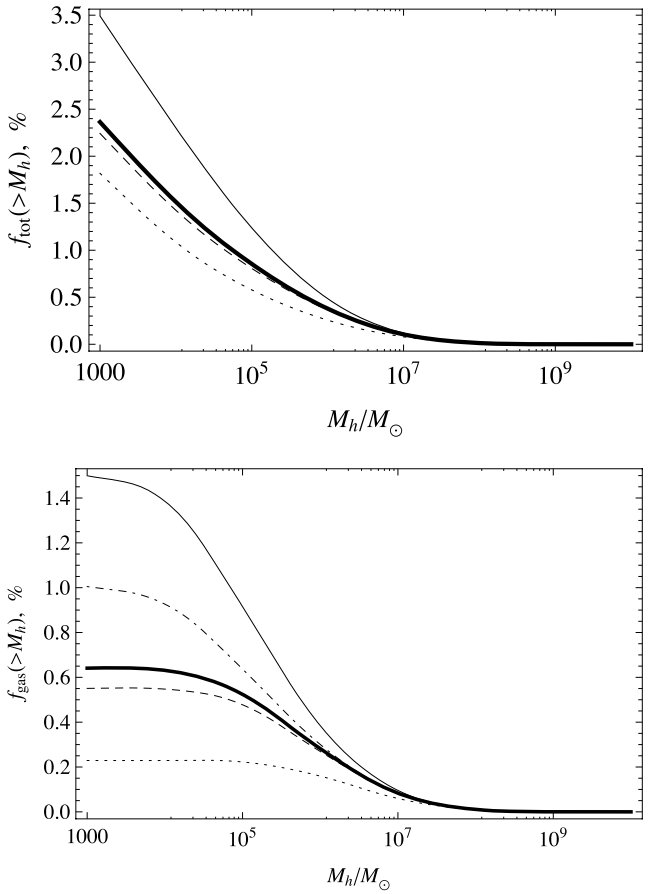

Figure 7. The mass fraction in haloes above M_h (upper panel) and the gas fraction in haloes (lower panel) at redshift $z = 20$ for the case $v_\mathrm{bc}/\sigma_\mathrm{vbc} = 0$ (thin solid line), 1 (dashed line), 2 (dotted line) and for the globally averaged case (thick solid line). In the lower panel, we show the case where we fix the value of M_F as calculated for $v_\mathrm{bc} = 0$ and use the correct globally averaged halo mass function including the variation with v_bc (dot–dashed line).

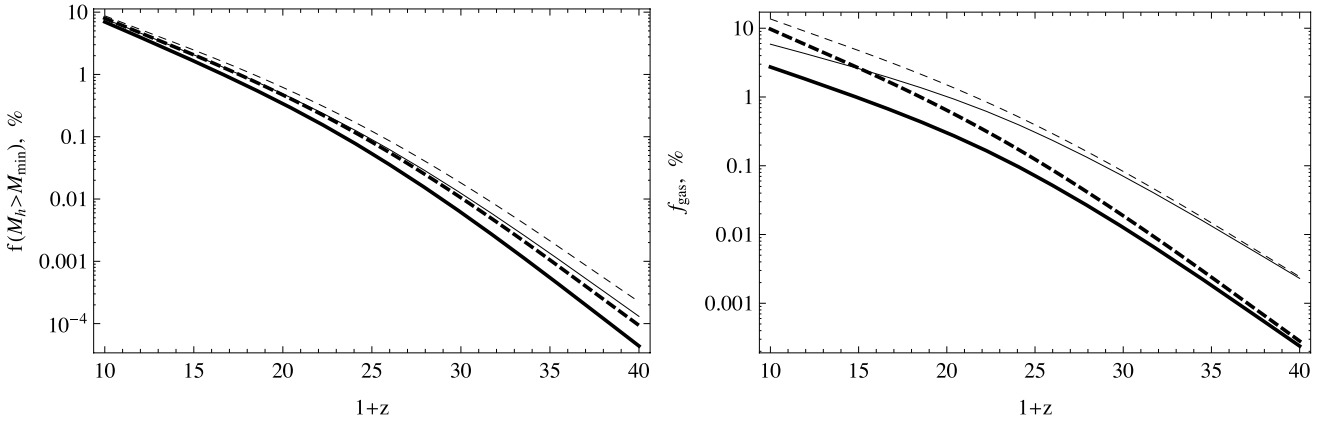

Figure 8. In the left-hand panel, we plot the total mass fraction in haloes above the cooling mass (dashed lines) and total gas fraction in haloes above the minimum cooling mass (solid lines). In the right-hand panel, we show the total gas fraction in haloes (dashed lines) and the total gas fraction in minihaloes, that is, in haloes below the minimum cooling mass (solid lines). All plots show two cases: no v_{bc} (regular lines) and the correct case where the v_{bc} effect is taken into account and isotropic averaging is performed (thick lines).

it varies with v_{bc}) but fix the filtering mass to the $v_{bc} = 0$ value. We find that the suppression arises from comparable contributions from the change in halo numbers and from the reduction in the internal halo gas fractions.

Stars are understood to form at high redshift out of gas that cooled and subsequently condensed to high densities in the cores of dark matter haloes. Since metals are absent in the pre-stellar Universe, the earliest available coolant is molecular hydrogen (H_2), and thus the minimum halo mass that can form a star is set by requiring the infalling gas to reach a temperature of several hundred Kelvin required for exciting H_2 to the $J \geq 2$ rotational levels (Tegmark et al. 1997). This has been confirmed with high-resolution numerical simulations containing gravity, hydrodynamics, and chemical processes in the primordial gas (Fuller & Couchman 2000; Abel, Bryan & Norman 2002; Bromm, Coppie & Larson 2002; Yoshida et al. 2003; Reed et al. 2005). These simulations imply a minimum halo circular velocity $V_c \sim 4.5\,\mathrm{km\,s^{-1}}$ for forming a star, where $V_c = \sqrt{GM/R}$ in terms of the halo virial radius R. The simulations show that in a halo above the minimum mass (which at $z = 20$ is $M_{min} \approx 6 \times 10^5\,M_\odot$), the gas cools in the dense centre and forms at least one star very quickly; this is understood theoretically since both the cooling time and the dynamical time are a small fraction of the cosmic age at that time. We are thus interested in the total gas fraction in haloes above this cooling threshold; if there is a fixed star formation efficiency in these haloes, then this gas fraction is directly proportional to the stellar density in each region.

We plot in Fig. 8 the evolution of various gas and total mass fractions as a function of redshift. Even without the relative velocity effect, there is a spatially-uniform suppression predicted for the gas fraction in haloes that can cool (i.e. a suppression of the overall star formation) by a factor of 1.2 at $z = 20$ and 1.5 at $z = 40$ (relative to the cosmic baryon fraction); this is due to the fact that the baryon perturbations are still catching up to the dark matter perturbations at these redshifts, even on large scales (beyond the filtering mass), and simulations suggest that non-linear halo formation amplifies the remaining differences (Naoz et al. 2010; Barkana & Loeb 2011). The relative velocity effect adds an additional suppression of cosmic star formation by a factor of 1.4 at $z = 20$ and 2.1 at $z = 40$. The relative velocities have a larger effect on the gas in minihaloes, the smaller haloes that accrete gas that cannot cool. Since the total mass fraction in haloes continues to increase as we consider smaller and smaller halo masses (Fig. 7), the total amount of gas in minihaloes is very sensitive to the filtering mass, which is what produces a gradual low-mass cut-off in gas accretion on to haloes. In the absence of the relative velocities, the total gas fraction in haloes at $z = 20$ is 1.5×10^{-2}, consisting of 1.0×10^{-2} in minihaloes and 5×10^{-3} in galaxies. At $z = 40$, these gas fractions are 2.4×10^{-5}, 2.3×10^{-5} and 1×10^{-6}, respectively. The relative velocities, in the global average, reduce these fractions to 6.4×10^{-3}, 3×10^{-3} and 3.4×10^{-3} at $z = 20$, and 2.8×10^{-6}, 2.4×10^{-6} and 4×10^{-7} at $z = 40$, respectively. Note that the gas fraction above the H_2 cooling mass is really an upper limit to the gas fraction that undergoes star formation. Any significant feedback effect will raise the effective threshold for star formation, making the total gas fraction in haloes to correspond almost completely to star-less haloes (see discussion in Section 4).

3.3 Probability distribution functions

In addition to plotting mean values of various quantities, it is interesting to consider their variation in different patches across the sky. Above, we have explicitly varied v_{bc} but averaged over the density fluctuations (note that the density and velocity are uncorrelated at a given point). However, in order to calculate the full amount of variation of different quantities, that is, the probability distribution function (PDF), we must explicitly vary both the mean density and the value of v_{bc} in each region.

In the absence of relative velocities, the extended Press–Schechter model gives the variation of the Press–Schechter halo mass function in regions of various mean density. No analytical generalization of this formalism is known for the more accurate Sheth–Tormen model, but Barkana & Loeb (2004) suggested a hybrid prescription that adjusts the abundance in various regions based on the extended Press–Schechter formula, and showed that it fits a broad range of simulation results. Generalizing this prescription to include the effect of relative velocity, we set

$$f_{\rm bias}(\delta_c(z), \bar{\delta}_{R_{\rm LS}}, R_{\rm LS}, M, v_{bc}) = \left[\frac{f_{\rm ST}(\delta_c(z), S'(R))}{f_{\rm PS}(\delta_c(z), S'(R))}\right] \times f_{\rm PS}\left(\delta_c(z) - \bar{\delta}_{R_{\rm LS}}, S'(R) - S'(R_{\rm LS})\right), \quad (22)$$

where the mean overdensity in the patch is $\bar{\delta}_{R_{\rm LS}}$, and for a given halo mass, the variance $S'(R)$ is calculated using the power spectrum modified by the local bulk velocity. The subtraction of $S'(R_{\rm LS})$ accounts for the fact that $\bar{\delta}_{R_{\rm LS}}$ arises from density modes on scales

larger than the patch size, leaving only the remaining variance $S'(R) - S'(R_{\rm LS})$ for fluctuation modes within the patch to supply the additional density needed to reach $\delta_{\rm c}(z)$ and thus form a halo. We clarify that the difference in variance is computed in a similar way to the variance from equation (16):

$$S'(R) - S'(R_{\rm LS}) = \int \Delta^2_{\rm m}(k, v_{\rm bc})(|W(k, R)|^2 - |W(k, R_{\rm LS})|^2)\frac{{\rm d}k}{k}, \quad (23)$$

where now $\Delta^2_{\rm m}(k, v_{\rm bc})$ is the isotropically averaged local matter power spectrum modified by the relative velocity effect.

In our case, the patches in which we will compute the baryon collapse fraction PDF will be spheres of radius $R_{\rm LS} = 3\,{\rm Mpc}$ (comoving). Note that if used to compute a mass function, the above formula gives the Lagrangian halo number density, while the Eulerian density is larger by a factor of $1 + \bar{\delta}_{R_{\rm LS}}$; however, no such transformation is necessary to compute the local *fraction* of gas in haloes.

We start by calculating the PDF for the filtering mass $M_{\rm F}$. In the scenario without $v_{\rm bc}$, we would have a universal value of $M_{\rm F}$; however, since various regions of space have different values of relative velocity of baryonic and dark matter fluids, this produces a variation in $M_{\rm F}$. The distribution of relative velocities is given by equation (13) and it translates into the distribution of $M_{\rm F}$ using

$$P_{M_{\rm F}}(M_{\rm F}) = P_{v_{\rm bc}}(v_{\rm bc})\frac{{\rm d}v_{\rm bc}}{{\rm d}M_{\rm F}}. \quad (24)$$

The PDF of the filtering mass at $z = 20$ and 40 is plotted in Fig. 9. These distribution functions are essentially determined by the distribution of the relative velocity and exhibit clear peaks which correspond to values of the filtering mass around the maximum of the $v_{\rm bc}$ distribution, which occurs at $v_{\rm bc} \approx 1.2\sigma_{v_{\rm bc}}$. As noted before (Figs 2 and 3), the filtering mass does not vary much in this redshift range, but at $z = 20$, it is slightly more sharply peaked, while the PDF at $z = 40$ extends more towards high values of $M_{\rm F}$. Filtering mass has a rather significant scatter with full width at half-maximum FWHM $\sim 1.5 \times 10^5\,{\rm M}_\odot$ at $z = 20$.

To better understand global properties of the first objects, we calculate PDFs of the total gas fraction in haloes as well as the gas fraction in haloes above the minimum cooling mass $M_{\rm min}$. As noted earlier, these gas fractions are affected by the distribution of relative velocities as well as the distribution of large-scale overdensities $\bar{\delta}_{R_{\rm LS}}$. We consider the PDF of gas fractions inside spherical patches

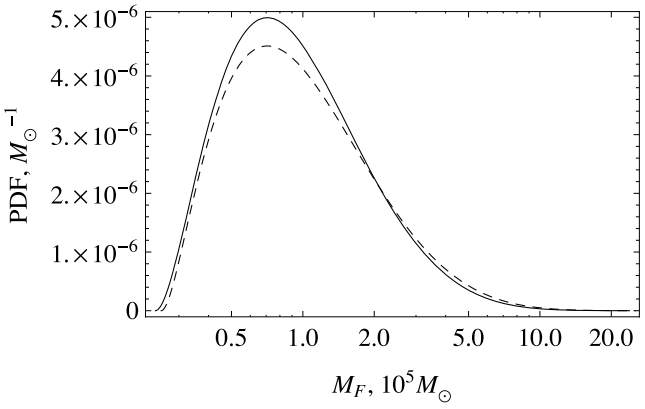

Figure 9. The PDF of the filtering mass $M_{\rm F}$ at $z = 20$ (solid line) and $z = 40$ (dashed line). We consider patches of radius $R_{\rm LS} = 3\,{\rm Mpc}$ and include the variation of $v_{\rm bc}$ as well as the mean density in each cell.

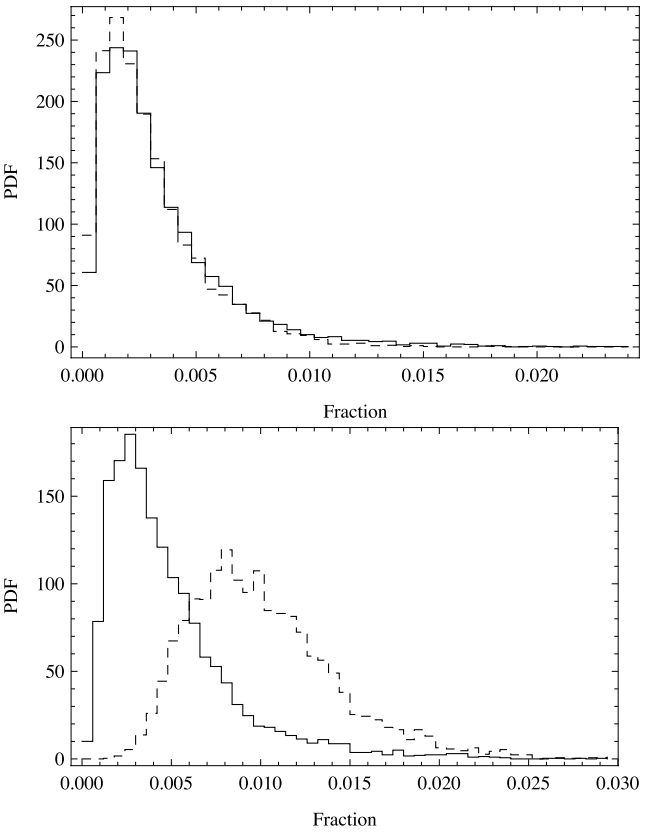

Figure 10. The PDFs of the gas fraction in haloes above the minimum cooling mass (solid line), and of the gas fraction in minihaloes, that is, haloes below the minimum cooling mass (dashed line) at $z = 20$ for the cases with the $v_{\rm bc}$ effect (upper panel) and without the effect (lower panel).

('cells') of radius $R_{\rm LS} = 3\,{\rm Mpc}$, which are small enough that $v_{\rm bc}$ can be treated as roughly constant over a cell. We obtain the PDFs by running a Monte Carlo simulation that generates random values of $v_{\rm bc}$ using equation (13) and of the large-scale overdensity within the cell $\bar{\delta}_{R_{\rm LS}}$ using a Gaussian of variance $S'(R_{\rm LS})$. In Fig. 10, we show the PDFs of the gas fractions in haloes above and below the minimum cooling mass $M_{\rm min} \approx 6 \times 10^5\,{\rm M}_\odot$ at $z = 20$. We also show the same distributions for the case with no $v_{\rm bc}$ effect. The figure shows how minihaloes would be dominant at $z = 20$ (by a factor of 2 compared to galaxies), but since $v_{\rm bc}$ has a larger effect on the minihaloes, it makes the gas content roughly equal between galaxies and minihaloes at that redshift. Each PDF has a non-Gaussian extension towards high fractions (in fact, the distribution is approximately lognormal). Thus, the peak of the PDF is significantly lower than the mean value; without the relative velocity, it is 0.002 for galaxies and 0.008 for minihaloes, and $v_{\rm bc}$ moves it to ∼0.0015 for both. Also, the relative velocities reduce the FWHM from 0.004 (galaxies) and 0.008 (minihaloes) to 0.003 for both.

4 CONCLUSIONS

We have shown that the relative velocity of baryons and dark matter has a significant impact on the properties of the first bound objects and has to be considered in detailed studies of the epoch of reionization and especially earlier epochs. The supersonic motion of the baryonic fluid relative to the underlying potential wells created by the dark matter causes advection of small-scale perturbations by

large-scale velocity flows, leading to a significant suppression of gas accretion during halo formation and dramatically increasing the characteristic mass of gas-rich objects at high redshifts ($z > 10$). In particular, instead of this characteristic filtering mass being close to the Jeans mass of $2 \times 10^4\,M_\odot$ at $z = 20$, it varies between various regions from this value up to $\sim 10^6\,M_\odot$, with a 1σ value (and global average) around $M_F = 2 \times 10^5\,M_\odot$, that is, an order of magnitude higher than without the relative velocity effect.

The relative velocity effect also modifies the star formation history, delaying star formation and causing significant spatial fluctuations. However, since the minimum mass for H_2 cooling ($\approx 6 \times 10^5\,M_\odot$ at $z = 20$) is somewhat higher than the average M_F, the suppression effect of v_{bc} is limited to about a factor of 1.4 at $z = 20$ (added on top of the spatially-uniform factor of 1.2 from the still-depressed baryon perturbations on large scales), compared to a much larger effect on the gas fraction in star-less gas minihaloes. The importance of the relative velocity grows steadily with redshift, so that at $z = 40$ the suppression factor for galaxies due to v_{bc} increases to 2.5 (on top of a pre-existing factor of 1.5).

In our detailed treatment, we included the spatial variation of the baryonic sound speed, the suppression of baryonic perturbations on large scales, and the effect of the relative velocity, through the modified power spectrum, both on the halo mass function and the internal gas fractions in haloes. In order to gauge the induced spatial variability, we further calculated the full PDFs of the characteristic mass and of gas fractions inside the first collapsed haloes. These results are important for understanding the relative velocity effect on large scales, and we plan to study them further.

Our results significantly extend the work done recently by Dalal et al. (2010). For example, we find a suppression factor due to v_{bc} at $z = 20$ of 1.4 and 3.3, for star-forming haloes and minihaloes, respectively. In their approach, Dalal et al. (2010) did not separate these two categories and found a factor of 2.5 suppression in the collapsed fraction, which under their approximation can be interpreted as a suppression of star formation. In our work, we removed this and many other approximations used in Dalal et al. (2010). Compared to our work, we expect that their calculation of Lyman α flux fluctuations is qualitatively correct but may be somewhat overestimated and requires a more detailed analysis.

As we were finishing this paper, two simulation papers appeared on the effect of v_{bc} at high redshift (Maio, Koopmans & Ciardi 2011; Stacy, Bromm & Loeb 2011). While both found a small suppression of star formation, their results appear at first glance to show a smaller suppression effect than we predict. This difference is not surprising if we note that these simulation papers focused on star-forming haloes around $z \approx 15$, while the largest effects that we find occur for star-less minihaloes at higher redshifts. At $z > 20$, Maio et al. (2011) find tens of per cents difference in the gas fractions, although the statistical errors are large. Stacy et al. (2011) find a delay in gas collapse by $\Delta a/a = 0.14$ for $v_{bc}/\sigma_{vbc} = 1$. We also note that the choice of initial conditions should be carefully considered: standard initial condition codes do not properly treat the separate baryonic and dark matter perturbations or the gas temperature perturbations, leading to a filtering mass that is too high by a factor of ~ 2 at $v_{bc} = 0$ (Naoz et al. 2010); as such they may underestimate the effect of relative velocities.

The simulations by Maio et al. (2011) and Stacy et al. (2011) clearly represent a very important step and will serve as a good foundation for simulations with larger boxes and improved initial conditions. Eventually, we hope that simulations including v_{bc} will advance to the point where improved fitting functions for the local halo mass function and gas mass fraction become available.

We note that various feedback effects may reduce or mask some of the effect of the relative velocity. For galaxies, local feedback from star formation may effectively raise the minimum halo mass for star formation (except for the very first generation of stars). The possibilities include supernova feedback as well as radiative feedback acting via photoheating and photoevaporation or suppression of H_2 formation, although 'positive' feedback due to X-ray ionization enhancing H_2 formation has also been suggested (Haiman, Rees & Loeb 1996, 1997). For minihaloes, astrophysical heating, for example, from an early X-ray background, may heat the gas and raise the filtering mass above the value due to v_{bc}. There are many unknowns, but these various effects could begin to be significant by $z \sim 20$, and very likely by the time of significant cosmic reionization. Still, the relative velocity between baryons and dark matter is the main determinant of the gas content of haloes at the highest redshifts.

ACKNOWLEDGMENTS

DT and CMH are supported by the US Department of Energy (DE-FG03-92-ER40701) and the National Science Foundation (AST-0807337). CMH is also supported by the David and Lucile Packard Foundation. RB is supported by Israel Science Foundation grant 823/09.

REFERENCES

Abel T. L., Bryan G. L., Norman M. L., 2002, Sci, 295, 93
Barkana R., Loeb A., 2002, ApJ, 578, 1
Barkana R., Loeb A., 2004, ApJ, 609, 474
Barkana R., Loeb A., 2011, MNRAS, 415, 44
Bennett C., et al, 2003, ApJS, 148, 1
Bond J. R., Cole S., Efstathiou G., Kaiser N., 1991, ApJ, 379, 440
Bromm V., Coppie P. S., Larson R. B., 2002, ApJ, 564, 23
Ciardi B., Scannapieco E., Stoehr F., Ferrara A., Iliev I., Shapiro P., 2005, MNRAS, 366, 689
Clark P. C., Glover S. C. O., Smith R. J., Greif T. H., Klessen R. S., Bromm V., 2011, Sci, 331, 1040
Dalal N., Pen U. L., Seljak U., 2010, J. Cosmol. Astropart. Phys., 11, 007
Eisenstein D., Hu W., 1998, ApJ, 496, 605
Fuller T. M., Couchman H. M. P., 2000, ApJ, 544, 6
Furlanetto S., Oh S. P., 2006, ApJ, 652, 849
Gnedin N. Y., 2000, ApJ, 542, 535
Gnedin N. Y., Hui L., 1998, MNRAS, 296, 44
Haiman Z., Rees M. J., Loeb A., 1996, ApJ, 467, 522
Haiman Z., Rees M. J., Loeb A., 1997, ApJ, 476, 458; erratum, 484, 985
Haiman Z., Abel T., Madau P., 2001, ApJ, 551, 599
Iliev I., Scannapieco E., Martel H., Shapiro P., 2003, MNRAS, 341, 81
Iliev I., Scannapieco E., Shapiro P., 2005, ApJ, 624, 491
Madau P., Meiksin A., Rees M., 1997, ApJ, 475, 429
Maio U., Koopmans L. V. E., Ciardi B., 2011, MNRAS, 412, L40
Naoz S., Barkana R., 2005, MNRAS, 362, 1047
Naoz S., Barkana R., 2007, MNRAS, 377, 667
Naoz S., Noter S., Barkana R., 2006, MNRAS, 373, L98
Naoz S., Barkana R., Mesinger A., 2009, MNRAS, 377, 667
Naoz S., Yoshida N., Barkana R., 2011, MNRAS, 416, 232
O'Shea B., Abel T., Whalen D., Norman M., 2005, ApJ, 628, L5
Press W. H., Schechter P., 1974, ApJ, 187, 425
Reed D. S., Bower R., Frenk C. S., Gao L., Jenkins A., Theuns T., White S. D. M., 2005, MNRAS, 363, 393
Seljak U., Zaldarriaga M., 1996, ApJ, 469, 437S
Sheth R. K., Tormen G., 1999, MNRAS, 308, 119
Sheth R. K., Tormen G., 2002, MNRAS, 329, 61

Stacy A., Greif T., Bromm V., 2010, AIP Conf. Ser. Vol. 1294, The First Stars and Galaxies: Challenges for the Next Decade. Am. Inst. Phys., New York, p. 289
Stacy A., Bromm V., Loeb A., 2011, ApJ, 730, 1
Tegmark M., Silk J., Rees M. J., Blanchard A., Abel T., Palla F., 1997, ApJ, 474, 1
Tseliakhovich D., Hirata C. M., 2010, Phys. Rev. D, 82, 083520
Yoshida N., Sokasian A., Hernquist L., Springel V., 2003, ApJ, 598, 73
Yoshida N., Omukai K., Hernquist L., 2008, Sci, 321, 669

This paper has been typeset from a TEX/LATEX file prepared by the author.